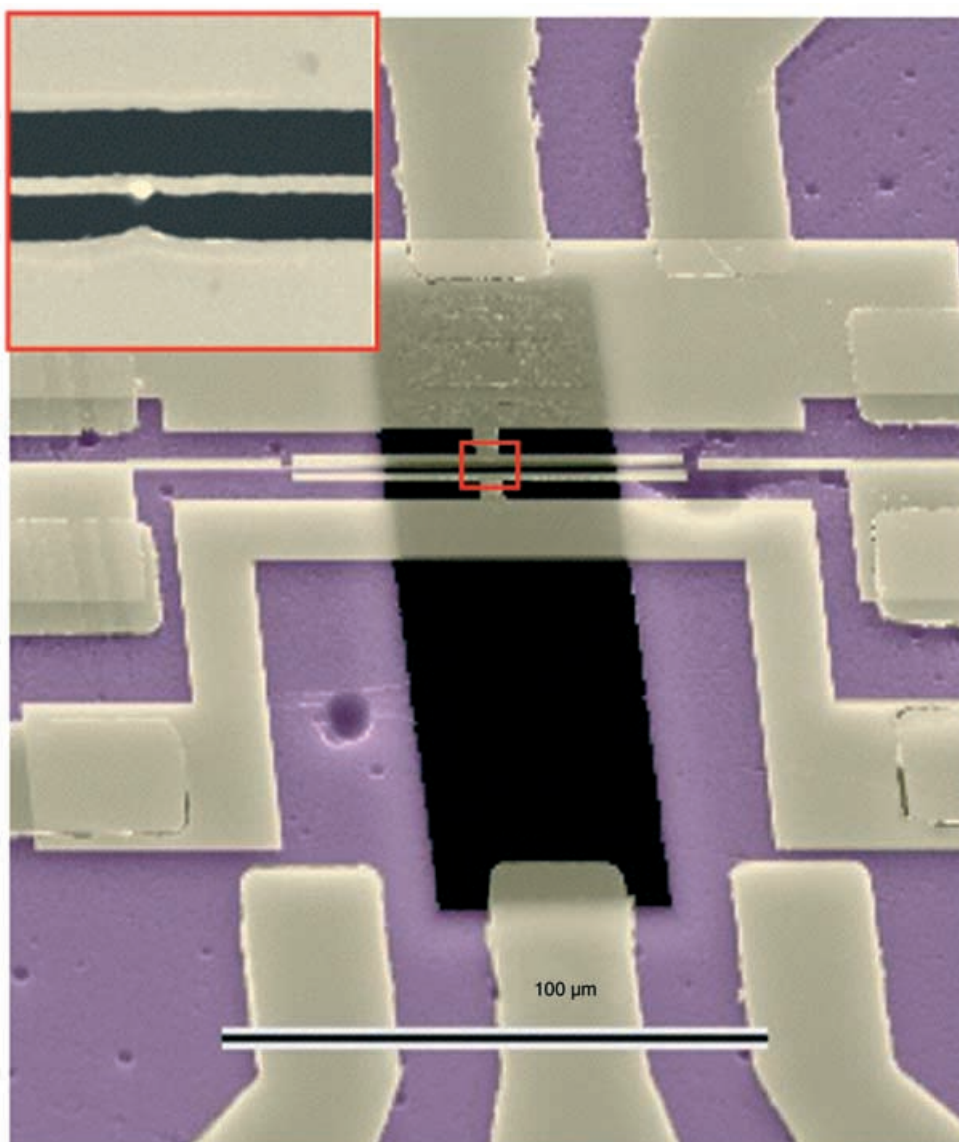


Electromechanical Transducers at the Nanoscale: Actuation and Sensing of Motion in Nanoelectromechanical Systems (NEMS)

*K. L. Ekinci**



SEM image of a nanoelectromechanical resonator integrated with two side gates for actuation and detection.

From the Contents

1. Introduction.....	787
2. Basic Concepts.....	788
3. Actuation of Motion in NEMS.....	789
4. Motion Detection.....	791
5. Summary and Outlook	795

Keywords:

- actuators
- nanoelectromechanical systems (NEMS)
- nanotechnology
- sensors

NANO MICRO
small

Electromechanical devices are rapidly being miniaturized, following the trend in commercial transistor electronics. Miniature electromechanical devices—now with dimensions in the deep sub-micrometer range—are envisioned for a variety of applications as well as for accessing interesting regimes in fundamental physics. Among the most important technological challenges in the operation of these nanoelectromechanical systems (NEMS) are the actuation and detection of their sub-nanometer displacements at high frequencies. In this Review, we shall focus on this most central concern in NEMS technology: realization of electromechanical transducers at the nanoscale. The currently available techniques to actuate and detect NEMS motion are introduced, and the accuracy, bandwidth, and robustness of these techniques are discussed.

1. Introduction

The terms “actuator”, “sensor”, and “transducer” are widely used in the description of measurement systems—sometimes interchangeably.^[1] In the broadest sense, a *transducer* receives energy from one system and transmits this energy to another system, often in a different form. A *sensor* monitors a system; it responds to physical stimuli, such as heat, light, pressure, or motion, and generates an electronic impulse for detection. An *actuator*, on the other hand, imposes a state upon a system. Most commonly, this

involves converting an input electrical impulse into motion. Thus, actuators and sensors are both transducers intended for different tasks. In accord with these general definitions, an *electromechanical transducer* converts electrical energy into mechanical energy, and vice versa.

An *electromechanical system* refers to a mechanical element coupled to electronic circuits via electromechanical transducers. Figure 1 illustrates a generic electromechanical device. The input transducer takes electrical signals from the input circuit and provides mechanical stimuli to the mechanical system; this is generally referred to as actuation. The response of the mechanical element—namely, its motion or displacement—is sensed by the output transducer, which generates electrical signals in the output circuit. These electrical signals in the form of currents and voltages can subsequently be measured. The overall purpose of this conversion of energy back and forth between the mechanical and electrical domains may be to accomplish a mechanical task in a controllable manner.

Electromechanical devices are ubiquitous in our daily lives in the form of loudspeakers, dishwashers, robot arms—the list goes on. Less familiar are the microscopic electromechanical systems that researchers have long been fashioning using the materials and processes of microelectronics. These micromechanical elements—beams, cantilevers, gears, and membranes—along with the enabling microelectronic circuits are called *microelectromechanical systems* (MEMS). MEMS perform a variety of tasks in present day technology, such as opening and closing valves, turning mirrors, and regulating electric current flow.

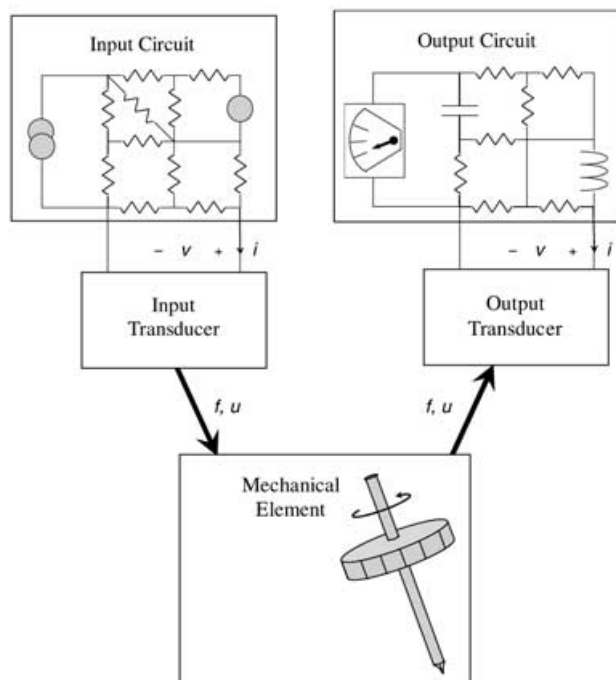


Figure 1. An electromechanical system: The input circuit actuates motion in the mechanical element via the input electromechanical transducer. The response of the mechanical element is transduced into measurable electrical impulses via the output transducers. Both transducers shown have electrical and mechanical ports.

[*] Prof. K. L. Ekinici
Department of Aerospace & Mechanical Engineering
Boston University, Boston, MA 02215 (USA)
Fax: (+1) 617-353-5866
E-mail: ekinici@bu.edu

With microelectronics technology now pushing deep into the sub-micrometer size regime, a concerted effort has surfaced to realize even smaller electromechanical systems: *nanoelectromechanical systems* (NEMS).^[2–4] Figure 2 shows

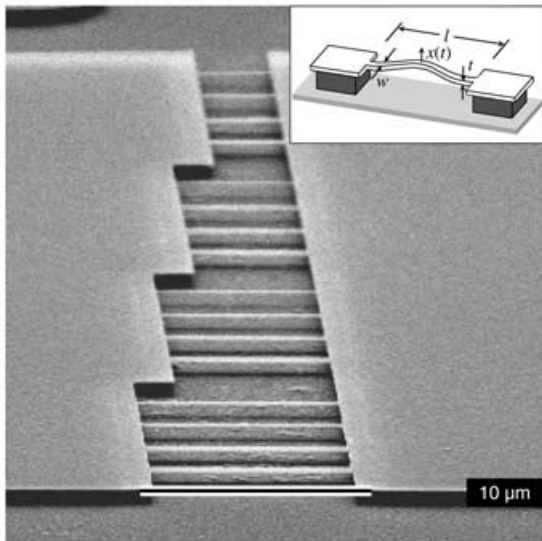


Figure 2. Scanning electron micrograph of doubly clamped NEMS beams, surface nanomachined out of B-doped silicon-on-insulator (SOI). The beams are patterned using electron beam lithography, metal deposition, lift-off, and various etching techniques. These doubly clamped beams have the following dimensions (inset): $3\ \mu\text{m} < l < 25\ \mu\text{m}$, $160\ \text{nm} < w < 1400\ \text{nm}$, $t = 219\ \text{nm}$. The fundamental out-of-plane flexural resonances of these beams were in the $15\ \text{MHz} < \frac{\omega_0}{2\pi} < 60\ \text{MHz}$ range.

silicon NEMS recently fabricated in the author’s laboratory. These are doubly clamped beams operated in their fundamental flexural resonant modes (inset)—much like simple tuning forks. In this size regime, NEMS offer access to frequencies in the microwaves,^[5] and mechanical quality (Q)



Kamil L. Ekinci has been an assistant professor in the Aerospace and Mechanical Engineering Department at Boston University since 2002. He obtained his PhD in physics from Brown University in 1999. There, he designed and built one of the first low-temperature scanning tunneling microscopes with sample manipulation capabilities. After obtaining his PhD, he joined the Condensed Matter Physics group at the California Institute of Technology

as a postdoctoral scholar with Prof. M. L. Roukes. During the years he spent at Caltech, he carried out research involving nanoelectromechanical systems (NEMS). At Boston University, his research group is currently focusing on nanomechanical sensors, integration of NEMS and photonic devices, and UHV scanning-probe microscopy. Ekinci is active in nanotechnology education at both the graduate and undergraduate levels, and has been involved in several nanotechnology outreach efforts.

factors in the tens of thousands^[6] with active masses in the picograms.^[7] This set of attributes translates into potentialities for a wide range of applications. Recent demonstrations of NEMS-based nanomechanical electrometry,^[8] signal processing,^[9,10] and mass detection^[7,11–13] have attracted much attention.

In this Review, we shall focus on arguably the most central concern in NEMS technology: realization of electromechanical transducers at the nanoscale. We shall introduce the currently available techniques to actuate and detect NEMS motion. There will also be a discussion of the accuracy, bandwidth, and robustness of these techniques and, in some cases, some proposed improvements.

2. Basic Concepts

Most recent NEMS are *resonant devices* (see Figure 2), where the nanomechanical element is excited in one of its resonant modes. This mechanical element in motion is sometimes also referred to as the “test mass”. A description of the system as a one-dimensional damped harmonic oscillator will be sufficient for our purposes here; the displacement $x(t)$ of this system follows the familiar equation

$$\ddot{x}(t) + \frac{\omega_0}{Q}\dot{x}(t) + \omega_0^2x(t) = f(t)/m_{\text{eff}} \quad (1)$$

Here, $f(t)$ is the driving force, m_{eff} is the effective mass, κ_{eff} is the stiffness, and Q is the quality factor of the mode in question. For a complicated mechanical structure, this one-dimensional approximation remains valid in the vicinity of a mode’s resonance frequency, as long as accurate lumped approximations are available for m_{eff} and κ_{eff} .

Most recent NEMS devices have been realized in the doubly clamped beam geometry. For the fundamental out-of-plane flexural mode resonance of the doubly clamped beam (see Figure 2), the effective mass, dynamic stiffness, and the resonance frequency are given as $m_{\text{eff}} = 0.735ltw\rho$, $\kappa_{\text{eff}} = 32Et^3w/l^3$, and $\omega_0 = 2\pi(1.05)\sqrt{E/\rho}(t/l^2)$, respectively.^[14] Here, $l \times t \times w$ are the dimensions, E is the Young’s modulus, and ρ is the mass density of the beam. When the center of the beam is displaced by a small distance x , the beam roughly lengthens by $\Delta l \approx x^2/l$ and its cross-sectional area A changes by $\Delta A \approx -\nu wtx^2/l^2$, where ν is Poisson’s ratio for the material. We also note that for $x \approx t/\sqrt{Q(1-\nu^2)}$, the linear description of motion in Equation (1) begins to fail.

Having defined the essentials of the mechanical element, we now turn to an electromechanical transducer. An electromechanical transducer is made up of an electrical port and a mechanical port. The transducer converts the voltage $v(t)$ and current $i(t)$ at its electrical port into a force $f(t)$ and velocity $u(t)$ at the mechanical port, and vice versa. In this rather general description, a 2×2 transfer matrix relates the parameters at the electrical and mechanical ports.^[15,16] The transfer matrix formalism has several advantages. It is straightforward to relate the power at the electrical port to the power at the mechanical port in terms of the matrix elements. Both an electromechanical actuator and a sensor, in

essence, can be described completely using the transfer matrix formalism. Another advantage is that when there are cascaded transducers, matrix multiplication suffices to produce the transfer matrix of the cascade. In some cases, however, the transfer matrix formalism might be redundant. There are also difficulties associated with formulating the matrix when the coupled circuits and mechanical systems are not trivial. Here, we shall not present a matrix formalism; instead, we shall focus upon the physical principles of transduction at the nanoscale.

When evaluating the effectiveness of an electromechanical transducer, it is customary to consider several key issues:

1) The *sensitivity* or the *resolution* of the transducer is of utmost importance. An electromechanical actuator intended for use in a NEMS device, for instance, ought to have the precision to apply small enough forces upon the nanomechanical element. On the other hand, a NEMS displacement sensor (along with the coupled detection circuit) should have low noise characteristics and large displacement responsivity. In most cases, this noise level will determine the limits of the displacement sensitivity. In other cases, when extremely low noise levels are achieved, fundamental fluctuations such as the thermomechanical displacement fluctuations in the mechanical element will set the operation limits. It is customary to express the displacement sensitivity in terms of a displacement noise with power spectral density $S_x(\omega)$. The defining relation for $S_x(\omega)$ follows from the fact that the rms noise power $\langle(\Delta x)^2\rangle = \langle(x - \langle x \rangle)^2\rangle$ can be expressed in terms of a (frequency-dependent) noise power density as^[17]

$$\langle(\Delta x)^2\rangle = \frac{1}{2\pi} \int_0^\infty S_x(\omega) d\omega \quad (2)$$

The brackets in the above expressions represent averaging.^[18] $S_x(\omega)$ has units of $\text{m}^2 \text{Hz}^{-1}$ and can be converted to a displacement by integration over the appropriate measurement bandwidth. We note that one can similarly define power densities for the voltage noise and the current noise in a circuit element or an amplifier.

2) A second important concept in the study of electromechanical transducers is *backaction*. Backaction describes the perturbation of the mechanical element by the sensor and the output circuit during the detection. In some sense, the displacement sensor actuates the mechanical element as electrical impulses are generated in the output circuit. Backaction noise, in this context, refers to the fluctuations induced in the mechanical element due to the noise in the electrical detection circuit or the transducer itself.

3) To couple into the motion of the mechanical element in ultrafast applications, for instance, to realize an ultrafast electromechanical system, a *broad transduction bandwidth* is essential. The available bandwidth is oftentimes determined by the coupled circuit.

4) When operating an electromechanical system, one usually desires to actuate and detect the motion of the me-

chanical element through separate transducers. *Orthogonality* of actuation and detection, that is, having transducers that strongly interact with the mechanical element, but with only weak direct couplings to each other, is another desirable property.

5) Finally, transducers that can be fabricated on the same chip as the mechanical element are referred to as *on-chip* or *integrated* transducers.

The mainstay electromechanical transducers in the domain of MEMS have been realized by exploiting electrostatic,^[19,20] piezoelectric,^[21] piezoresistive,^[22] magnetic,^[23] and optical^[24,25] phenomena. In free-space optical MEMS devices, optical interferometry^[26–28] and optical beam deflection^[29,30] have been used efficiently. More recently, integrated micro-opto-electromechanical systems (MOEMS) have emerged, in which light is guided in moving optical waveguides rather than in free space.^[31–33]

As a mechanical device becomes smaller, its range of motion diminishes in direct proportion to its size. This necessitates actuation and detection of sub-nanometer displacements in most NEMS. Most transduction techniques from the domain of MEMS quickly reach their limits when carried over to the reduced dimensions of NEMS: some lose sensitivity; others lack speed (bandwidth). While in some cases stray couplings and embedding parasitic impedances are to blame, in other cases the physical phenomena of transduction is just not compatible with the reduced length scale of NEMS.

3. Actuation of Motion in NEMS

We first turn to actuation of motion in NEMS. There are two techniques that are used extensively: magnetomotive and capacitive (electrostatic) actuation. There are several other techniques that have not been fully explored, but may be of importance for next-generation NEMS.

3.1. Magnetomotive Technique

In magnetomotive motion actuation, the Lorentz force generated upon a current-carrying conductor in a static magnetic field supplies the actuation force.^[34] The scheme is illustrated in Figure 3 in a doubly clamped NEMS beam. Here, one drives an ac current at frequency ω through the beam in the presence of a strong magnetic field. Depending upon the orientation of the nanomechanical beam element with respect to the magnetic field, the actuation force can be applied in the in-plane or out-of-plane direction. The force acting upon the beam (expressed in the Fourier transform domain) is $F(\omega) = lBI(\omega)$, where $I(\omega)$ is the magnitude of the harmonic drive current, l is the length of the beam, and B is the magnetic field strength. The harmonic displacement of the center of the beam can be expressed as

$$X(\omega) = \frac{lBI(\omega)}{m_{\text{eff}}\left(\omega_0^2 - \omega^2 + \frac{i\omega\omega_0}{Q}\right)} \quad (3)$$

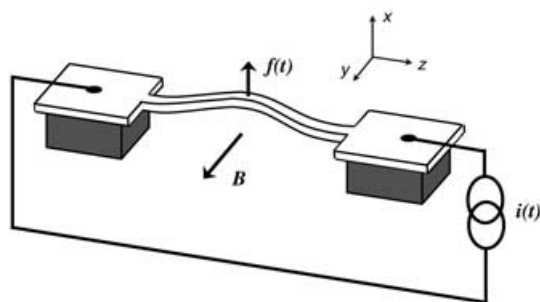


Figure 3. Magnetomotive actuation scheme: The NEMS beam is placed in a magnetic field and an ac current at frequency ω is forced through the beam by a current source. The Lorentz force generated in the out-of-plane direction (x -axis) actuates the motion. Alternatively, by applying a magnetic field along the x -axis, in-plane motion can be actuated.

Magnetomotive actuation technique is broadband, even in the presence of parasitic capacitances. Recently, magnetomotive actuation of NEMS at ≈ 1 GHz has been demonstrated by Huang et al.^[5] The only drawback is the requirement of strong magnetic fields, which are usually generated by using superconducting coils.

3.2. Electrostatic (Capacitive) Actuation

This technique has been carried over from the MEMS domain. An attractive force develops between the plates of a capacitor when the plates are charged. To realize electrostatic actuation, one usually fabricates a gate electrode in the vicinity of the NEMS device, as shown in Figure 4. Alternatively, the electrostatic potential can be applied through the substrate. Various degrees of complexity can be introduced in modeling capacitive actuators, as has been done in the domain of MEMS.^[35,36] In capacitive actuation, the capacitance of the actuation gate will be in parallel with the parasitic capacitance on the chip, which is many orders of magnitude larger than the gate capacitance. This in effect will reduce the efficiency of actuation at high frequencies. Nevertheless, the work of Craighead and co-workers has shown that electrostatic actuation in NEMS works reliably at frequencies as high as 700 MHz.^[37]

3.3. Other Techniques

Other interesting techniques of NEMS actuation have been proposed and demonstrated, but the full potential of these techniques is yet to be explored. Thermal actuation is one technique that bears significant potential. In the MEMS domain, thermal actuation has been realized by using bilayer structures with different thermal expansion coefficients. The bilayer structure, when heated, is subjected to stresses due to the differential thermal expansion between the layers. A structure can be designed to realize actuation in a certain mode or plane. The bandwidth of such techniques depends upon the thermal time constant τ_T of the structures,

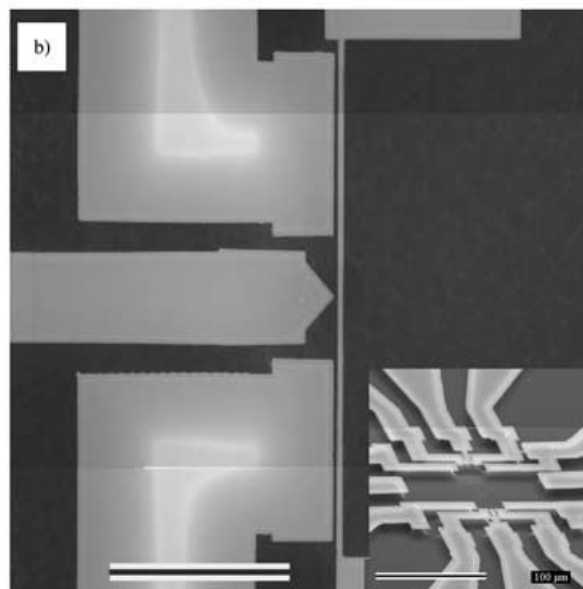
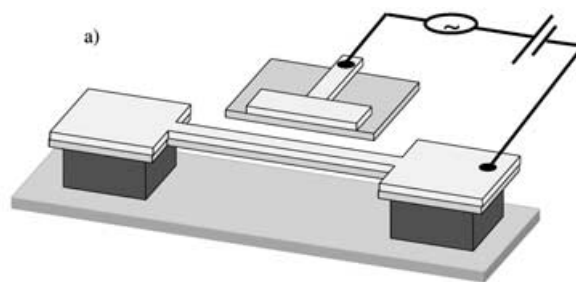


Figure 4. a) Electrostatic actuation in NEMS. A gate electrode is fabricated near the NEMS device and a voltage is applied bias between the gate electrode and the device. The actuation force depends nonlinearly upon the excitation voltage and will have components present at higher harmonics. To get a large contribution at the drive frequency, a voltage that has a large dc and a small ac component is usually applied. b) A device from the author's laboratory that has two gates fabricated in the close proximity to a doubly clamped beam. Scale bar = 10 μm (C. C. Huang and K. L. Ekinci, unpublished results).

given that the structure has to cool down and return to its initial shape before the next pulse of heat arrives. In small structures such as NEMS, τ_T is small, in the $1 \text{ ps} \leq \tau_T \leq 1 \text{ ns}$ range. This indicates that thermal actuation can be employed in small, high-frequency NEMS. The challenge is in efficiently delivering the heat pulse to the structure. One feasible approach is to use heating effects of radiation. A laser pulse, for instance, is ideal for such a task.

Piezoelectricity encountered in some materials is another unexplored phenomenon with potential in the nanoscopic domain. A piezoelectric material responds to an externally applied electric field by deforming—called the “inverse effect”. Much like thermal actuation, the bandwidth of a piezoelectric actuator depends upon the relaxation time of the deformations after the electric field is removed. In this respect, the RC time or the charging time of the actuation circuit is likely to dominate rather than the microscopic relaxation time of the crystal. Magnetostriction, the dimen-

sional change of a magnetic material resulting from a change in its magnetic state, is similarly an unexplored phenomenon for NEMS actuation.

4. Motion Detection

The detection of displacements at the nanoscale is a significantly more challenging task than actuation. The miniscule displacement amplitudes in NEMS necessitate displacement transducers with extremely high sensitivities. Given that NEMS devices are intended for use in ultrafast applications, a large transduction bandwidth is essential. The currently available techniques are reviewed below. At the end of this discussion, it will be clear that robust, broadband, and sensitive displacement detection schemes for NEMS are much needed.

4.1. Magnetomotive Technique

Cleland and Roukes introduced the magnetomotive displacement detection technique^[38] into the NEMS domain in 1996.^[34] The scheme is based upon the presence of a uniform static magnetic field, through which a conducting nanomechanical element is moved. The time-varying flux generates an induced electromotive force (emf) in the loop, which, in turn, can be picked up by the detection circuit. For a doubly clamped beam (see Figure 3), the magnetomotive technique generates an emf given by

$$v_0(t) = \xi l B \dot{x}(t) \quad (4)$$

Here B is the magnetic field strength, l is the length of the beam, and ξ is a geometric factor ($\xi \approx 0.885$ for a doubly clamped beam). As usual, $x(t)$ is the displacement of the midpoint of the beam; we shall assume that the beam exhibits constant amplitude harmonic oscillations at a frequency ω . Given the extremely small displacements and, hence, the small emf, one almost always uses a low-noise amplifier to boost the signal. We illustrate the magnetomotive transducer coupled to an amplifier in Figure 5. We have used a standard amplifier model with two uncorrelated noise sources: a voltage and a current noise source with respective power spectral densities $S_V(\omega)$ and $S_I(\omega)$. In most

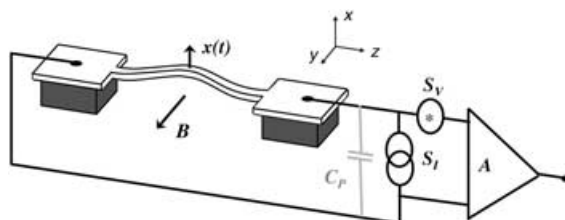


Figure 5. Magnetomotive displacement detection: The displacement sensitivity in the text is estimated by assuming that the dominant source of noise is the noise generated in the amplifier. The detection bandwidth will be affected by the parasitic capacitance shown in gray.

applications, the noise power generated in the amplifier determines the displacement sensitivity as

$$[S_X(\omega)]^{1/2} = \left(\frac{S_V(\omega)}{(\xi l B \omega)^2} + \frac{S_I(\omega) l^2 B^2}{m_{\text{eff}}^2 (\omega_0^2 - \omega^2)^2 + \frac{\omega^2 \omega_0^2}{Q^2}} \right)^{1/2} \quad (5)$$

Consider the two terms on the right hand side of Equation (5). The first term, namely the voltage noise in the amplifier, obscures the displacement as long as it is greater than the physical displacement converted to a voltage. Remember that the conversion factor, that is, responsivity of the scheme, is $\xi l B \omega$ (see Equation (4)). The second term has a more subtle physical interpretation: the current noise in the amplifier flows into the NEMS beam and drives the beam with a fluctuating force (see the discussion on magnetomotive actuation in Section 3.1). This adds up to the observed displacement noise at the amplifier output. In this respect, the current noise in the amplifier is the source of the backaction force noise discussed above. With a modest rf amplifier, one can achieve a displacement noise floor approaching $10^{-4} \text{ nm Hz}^{-1/2}$ for a $1 \mu\text{m}$ long beam vibrating at 1 GHz in a 10 T magnetic field.

The detection bandwidth in the magnetomotive technique will most likely be limited by the parasitic capacitances in the detection circuit. The emf develops across the NEMS beam (see Figure 5) and hence, the source impedance for the signal is the electrode resistance R_e . In metalized NEMS $R_e \approx 100 \Omega$, which implies a detection bandwidth greater than 1 GHz for a $\approx 1 \text{ pF}$ parasitic capacitance.

There are difficulties associated with implementing the magnetomotive detection scheme when the device is being actuated electrically, that is, by magnetomotive or electrostatic actuation. The parasitic coupling between the input and the output reduces the degree of orthogonality of the actuation and detection. A solution is to implement a reflection measurement scheme.^[34,39] The reflection technique, in turn, suffers from large background signals in smaller, high-frequency devices. A balanced bridge technique has recently been developed to remedy some of the limitations in reflection measurements.^[6]

4.2. Optical Techniques

Recently, optical interferometry techniques, in particular path-stabilized *Michelson interferometry* and *Fabry-Perot interferometry*, have been extended into the NEMS domain.^[40-44] In path-stabilized Michelson interferometry, a tightly focused laser beam reflects from the surface of a NEMS device in motion and interferes with a stable reference beam. In the case of Fabry-Perot interferometry, the optical cavity formed within the sacrificial gap of the NEMS—between the NEMS surface and the substrate—modulates the optical signal on a photodetector as the NEMS device moves in the out-of-plane direction. Figure 6 displays schematic diagrams of free-space optics to implement these techniques.

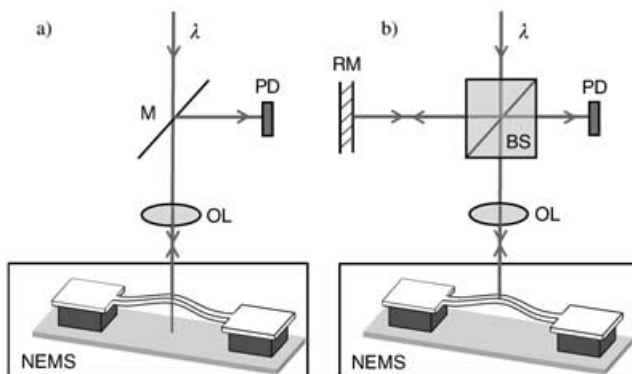


Figure 6. Optical displacement detection in NEMS: A probing laser beam of wavelength λ is focused upon the center of a doubly clamped beam through an objective lens (OL). a) In Fabry-Perot interferometry, the reflected light from the NEMS structure is collimated through the same lens and is directed onto a photodiode (PD). b) In Michelson interferometry, the light from the device interferes with a reference beam created using a beam-splitter (BS) and a reference mirror (RM).

In both of the above-described techniques, strong diffraction effects emerge as the relevant NEMS dimensions are shrunk beyond the optical wavelength used. The light collected by the probing lens is reduced to a small fraction of the incoming light due to strong scattering. In Figure 7, a Gaussian-profile probe beam incident upon a sub-wavelength NEMS is shown, along with numerical simulations of the light scattered by the structure. This strong scattering, coupled with the requirement that low optical power levels must be used for probing NEMS, makes optical displacement detection a relatively insensitive technique for the smallest devices. Shot noise limited displacement sensitivities demonstrated on larger objects, such as AFM cantilevers,^[45] are not easily achievable on NEMS.

Optical integration might offer prospects for optical displacement detection in NEMS. The concept of integrated optics has been known for over 35 years, first through the publications of Marcatili^[46] and Goell,^[47] who presented a complete method of waveguide analysis and designs for filters and waveguide bends. More recently, optically integrated MEMS, otherwise known as MOEMS, have emerged where light is guided in moving optical waveguides, rather than in free space.^[31–33] Applications of waveguide-based MOEMS extend to pressure,^[48] vibration, and acceleration sensors,^[49] as well as optical switches.^[50] A variety of materials such as GaAs/AlGaAs,^[51] and silicon-on-insulator (SOI)^[52,53] has been used. The minimum size of such a waveguide device depends upon the index differences of the layers forming the waveguide, that is, $\Delta n = n_1 - n_2$. Typical systems, such as optical fibers, have $\Delta n \approx 0.01$ and cross-sectional dimensions, $t \times w \approx 10 \mu\text{m} \times 10 \mu\text{m}$. Larger contrast leads to reduced dimensions as the confinement in the high dielectric material improves. In Si/SiO₂, where $\Delta n \approx 2$ at $\lambda \approx 1.5 \mu\text{m}$, single-mode devices with dimensions as small as $t \times w \approx 250 \text{ nm} \times 400 \text{ nm}$ have been operated.^[54] Thus, a suspended nanoscale waveguide could be operated as an optically integrated NEMS device. In this scheme, one would

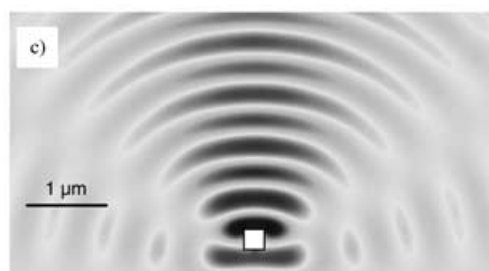
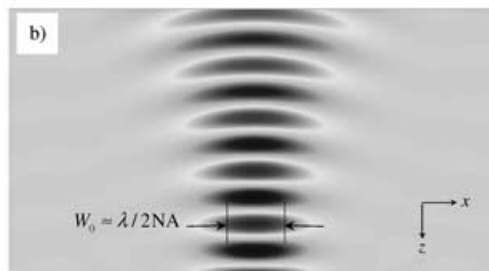
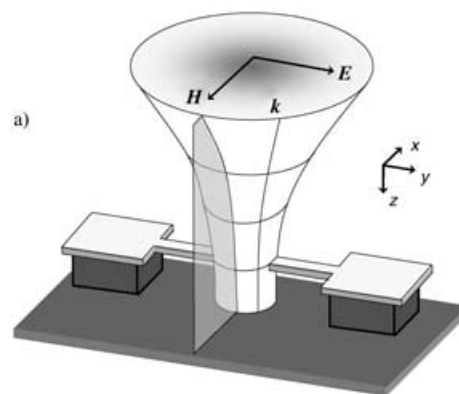


Figure 7. a) Illustration of a TE-polarized (i.e., electric field out of plane), collimated Gaussian beam focused onto a NEMS through an objective lens. b) A plot of the electric-field amplitude of the incoming Gaussian in the xz plane passing through the center of the beam. Here, $\lambda = 632 \text{ nm}$ and the beam is focused by an objective lens with numerical aperture $NA = 0.5$, and focal length $f = 4 \text{ mm}$. c) The electric field amplitude of the reflected-scattered EM field from the NEMS beam. In this two-dimensional finite element model, the beam had width $w = 170 \text{ nm}$, thickness $t = 200 \text{ nm}$; the sacrificial layer thickness between the beam and the substrate was 300 nm . The substrate is positioned at the bottom. (D. Karabacak, T. Kouh and K. L. Ekinci, unpublished results).

couple the light into the waveguide from one end, actuate motion of the waveguide, and detect phase shifts in the light coming out. Measurable phase shifts would be induced by changes in the optical path length, $\Delta = (n_{\text{eff}}l)$. Here, n_{eff} is the effective refractive index, and l is the waveguide NEMS length.

To clearly assess the feasibility of optically integrated NEMS, detailed modeling is needed. Another challenge in integrated waveguide technology is the efficient coupling of

light from a fiber into a sub-micrometer waveguide. For a lensed fiber, for instance, using simple modal overlap considerations, one obtains less than 1% coupling efficiency into a nanoscale Si waveguide. Moreover, energy losses due to scattering from surface defects are enhanced in small waveguides. Relatively large optical power losses^[55] as high as 40 dB cm^{-1} have been reported in sub-micrometer waveguides, primarily due to surface roughness.^[56–58]

4.3. Capacitive Displacement Detection

In capacitive displacement detection, the motion of the mechanical element modulates the electrical capacitance between the element and a fixed gate. To detect this capacitance modulation, one current (voltage) biases the capacitor, and looks for a change in the voltage (current flow) across the capacitor. It is straightforward to see from the definition of capacitance, $C = Q/V$, that $dQ = VdC + CdV$. Consequently, a capacitance change at constant current (voltage) will generate a voltage (current flow) across the capacitor. Here, Q is the charge on the capacitor and V is the voltage across it. Figure 8 shows an implementation

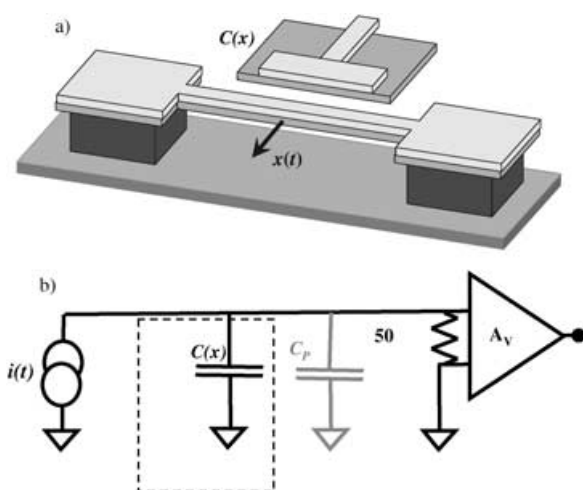


Figure 8. Capacitive displacement detection: a) Implementation of capacitive detection in a doubly clamped NEMS beam. The capacitance between the beam and the electrode depends upon the position of the beam center. b) If the junction is current biased, for instance, a capacitance change due to motion will result in current flow into the amplifier. The parasitic capacitance C_p , however, reduces the effective bandwidth.

along with a conceptual detection circuit. The parasitic element (shown in gray) in this current biased capacitor will be extremely important in determining the limits of capacitive detection of motion.

At the scale of MEMS, the dynamical capacitance changes due to motion are usually in the 10^{-9} – 10^{-12} F range. Such changes are readily detectable at the typically low operation frequency range of these devices. In the domain of NEMS, however, typical capacitance modulations are in the 10^{-16} – 10^{-18} F range, while the unavoidable parasitic capaci-

tance C_p of the chip and the embedding circuitry may be many orders of magnitude larger. Consequently, the displacement signals are divided between the device and the sensing amplifier. The scaling of capacitive detection into the nanoscale, therefore, requires delicate engineering.

A solution would be to eliminate the effect of the large embedding parasitic impedances. To this end, balanced bridge techniques may help readout the small dynamic capacitance changes efficiently by negating the capacitive background. Impedance matching techniques might also offer remedies.^[59] One could also locate the subsequent amplification stage directly at the capacitive transducer. Recently, a single-electron transistor (SET) has been integrated to a NEMS resonator^[60,61] with the NEMS electrode serving a dual purpose as both the motion sensor for the NEMS, and as the gate electrode of the SET readout.^[62,63] Using this approach, Schwab and co-workers have recently achieved a displacement sensitivity of $\approx 4 \text{ fm Hz}^{-1/2}$ —close to the quantum limit of a NEMS resonator.^[60] In their scheme displayed

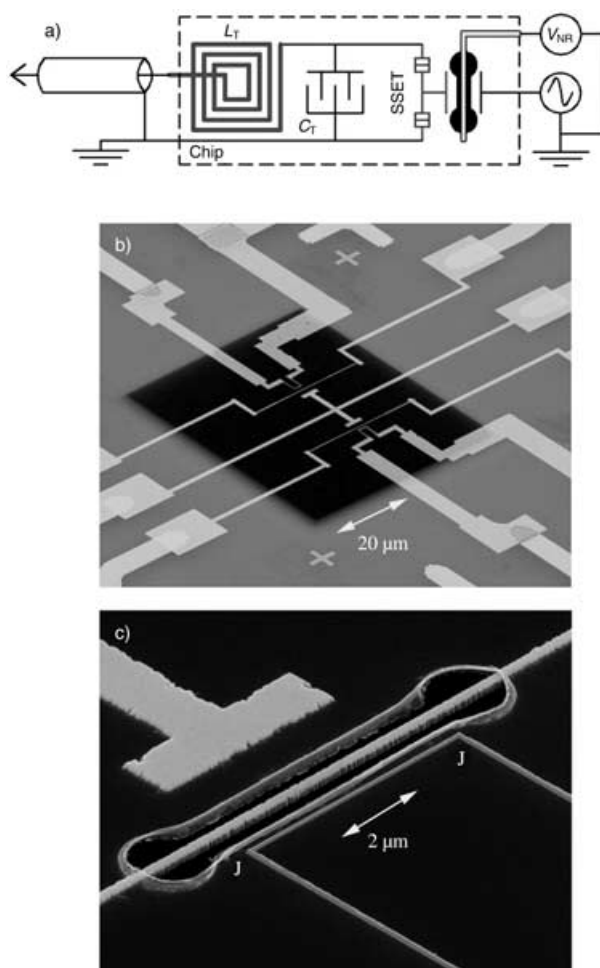


Figure 9. Capacitive displacement detection with a single-electron transistor (SET): a) Schematic showing a nanomechanical beam biased with a constant voltage, so that its in-plane flexural motion changes the charge coupled to a nearby SET. The conductance changes through the SET are efficiently read out at high frequencies by means of a resonant LC circuit. b, c) The fabricated structure (reproduced from ref. [60]).

In Figure 9, the nanomechanical beam is biased with a constant voltage, so that its in-plane flexural motion changes the charge coupled to a nearby SET. This, in turn, changes the measured current through the SET.

4.4. Piezoresistive and Piezoelectric Detection

Both piezoresistive and piezoelectric detection are sensitive to the strains generated inside a material during motion rather than the actual displacement itself. A material that exhibits a change in resistivity due to strain is called piezoresistive. Similarly, a piezoelectric material becomes electrically polarized in the event of a deformation.

Piezoresistive sensing can be realized by detecting the resistance changes through a piezoresistive NEMS device as it is actuated. There are, however, some challenges in this approach. In a p-type Si doubly clamped beam, for instance, an optimistic estimate^[64] for the resistance change ΔR , as a function of the displacement, the beam length l , and the resistance R , is $\Delta R/R \approx x^2/l^2$ —indicating that $\Delta R_{\max}/R \approx 1/100$. Coupled with the already high resistance of a doped semiconductor beam approaching $R \approx 10 \text{ k}\Omega$,^[6] such a small resistance change will be obscured at high resonance frequencies in the presence of parasitics.

In the piezoelectric scheme,^[65] one exploits the polarization fields created by the strain fields within the piezoelectric nanomechanical element as it moves. The detection is then realized by very sensitively measuring the potential drop across the strained device. In most materials, the piezoelectric coefficients that link the strain to the polarization field are $\approx 10^{-12}$ – 10^{-9} m V^{-1} —indicating that the piezoelectric voltage generated across a nanoscale device will be very small.^[14] This fact coupled with the high source impedance of the generated (piezoelectric) signal will make detection challenging at high frequencies. Cleland and co-workers have proposed piezoelectric detection in NEMS using a single-electron transistor (SET).^[66] Their proposed scheme is depicted in Figure 10. Here, the gate of the SET is placed at a position of maximum strain, and detection is realized by monitoring the resulting conductance changes in the current-biased SET.

4.5. Electron Tunneling

The tunneling transducer is generally realized in the form of a sharp tip placed within a fraction of a nanometer of the moving mechanical element.^[67] By drawing a tunneling current from the surface of the mechanical element, the tip converts $x(t)$ into an electrical signal. A tunneling transducer followed by a trans-impedance amplifier (current-to-voltage converter) is illustrated in Figure 11.

In the simplest, one-dimensional description, the tunnel current i through the junction is related to the dc bias voltage V and the tunnel gap d as $i \approx \rho_S(E_F) V e^{-2\kappa d}$.^[68] There are two important quantities that determine the transduction characteristics: $\rho_S(E_F)$ and κ . The latter, κ , is the decay constant for the electron wave-function within the gap and

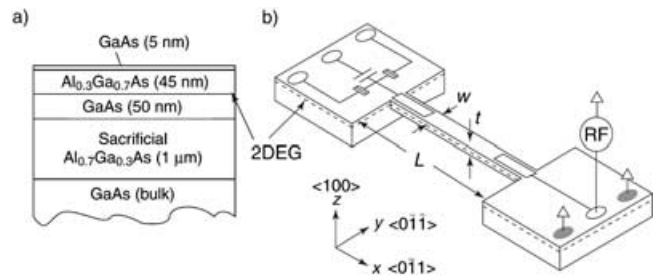


Figure 10. a) GaAs/AlGaAs heterostructure design for piezoelectric displacement detection. The layer thicknesses are indicated in parentheses. A two-dimensional electron gas (2DEG) is formed at the GaAs–Al_{0.3}Ga_{0.7}As interface. The 2DEG acts as a ground plane for the actuation and detection signals. b) Sketch of a nanomechanical doubly clamped beam with a SET situated at one end of the beam, coupled to a detection electrode. The second electrode, driven by a radio frequency source at the other end, is for piezoelectric actuation. The GaAs crystal axes, and the geometric axes, are indicated. Flexure of the resonator in the z direction, with the (100) crystal axis aligned along the z direction, will generate a piezoelectric polarization density along z . The polarization amplitude will be proportional to the distance from the midpoint of the beam. The polarization induces a screening charge on the detection electrode, which can subsequently be detected by the SET (reproduced from ref. [66]).

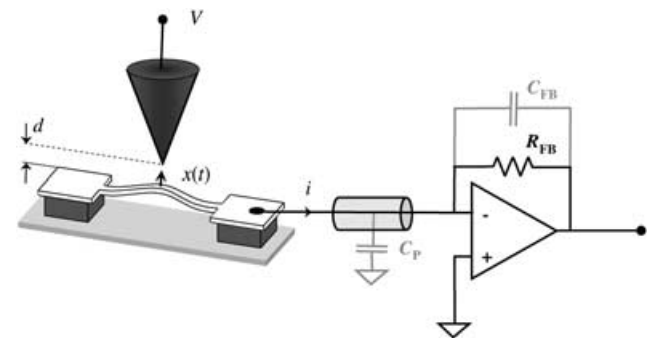


Figure 11. Tunneling transducer for displacement detection in NEMS. The tip is kept at a higher potential than the NEMS surface, which is at virtual ground. The trans-impedance amplifier generally has a large feedback resistor R_{FB} for a large signal-to-noise ratio. The parasitic capacitances determine the bandwidth limits.

$\kappa = \sqrt{2m_e\phi}/\hbar$; here, m_e is the mass of the electron, ϕ is the approximate work function of the metal and \hbar is Planck's constant divided by 2π . $\phi \approx 3$ – 5 eV and $\phi \gg eV$ in most cases. Using typical values, one can determine that $\kappa \approx 0.1 \text{ nm}^{-1}$. The former quantity, $\rho_S(E_F)$, is the local density of electronic states in the test mass. For $V \ll E_F$ where E_F is the Fermi energy of the metal in question, $\rho_S(E_F)$ can be assumed to be voltage-independent.

Given the exponential dependence of i upon the tunnel gap and the fact that $\kappa \approx 0.1 \text{ nm}^{-1}$, it is clear that a tunneling transducer will be extremely sensitive to the displacement of the mechanical element. It is assumed that the junction is biased at a dc current value I and very small displacements modulate the current as $i \approx I + \delta i(x)$. One can obtain a linearized current responsivity as $|\delta i/\delta x| \approx 2\kappa I$. Using this responsivity, it is possible to convert the various sources of

noise in the measurement into a limiting displacement noise floor:^[69–71]

$$[S_x(\omega)]^{1/2} = \left(\frac{S_I^{(A)}(\omega)}{4\kappa^2 I^2} + \frac{e}{2\kappa^2 I} + \frac{S_F^{(BA)}}{m_{\text{eff}}^2(\omega_0^2 - \omega^2)^2 + \frac{\omega^2 \omega_0^2}{Q^2}} \right)^{1/2} \quad (6)$$

The first term on the right hand side is due to the equivalent current noise of the trans-impedance amplifier—usually in the $S_I^{1/2} \approx 10^{-13}$ A Hz^{-1/2} range. The second term arises from the granular nature of the electronic charge: the shot noise current power density at high temperature is given by $S_I^{(S)} \approx 2e\langle i \rangle \approx 2eI$. For a typical tunnel current of 1 nA, $[S_I^{(S)}]^{1/2} \approx 10^{-14}$ A Hz^{-1/2}. The nature of the backaction force noise due to the tunneling electrons has been a topic of active research.^[70,72–78] Electrons tunneling into the test mass have finite momentum and each electron—regarded here as a particle—does impart this momentum to the test mass. The total impulse per unit time determines the back action force, that is, $f = Ip/e$. Here, p is the momentum of a single electron. To determine the noise in the transducer, the fluctuating component of this backaction force is required. The shot noise in the current creates a component of the backaction force noise that has spectral density $(p/e)^2 2eI$. In addition, each tunneling electron, due to the spread of its wavefunction across the tunnel junction, possesses a momentum uncertainty. The position uncertainty of a tunneling electron is $\Delta x \approx d \approx 1/\kappa$. The momentum uncertainty then becomes $\Delta p \approx \hbar/\Delta x \approx \hbar\kappa$. The variance (or the fluctuations in the force) is $\Delta f \approx (\hbar\kappa)I/e$ —given that force is the temporal rate of change of impulse. To find a rough approximation for the spectral density of the force noise based upon Equation (2), we divide $(\Delta f)^2$ with the effective bandwidth $\Delta\omega \approx I/e$. The spectral density of the backaction force noise then becomes:^[69,70]

$$S_F^{(BA)} \approx (\hbar\kappa)^2 \frac{I}{e} + \left(\frac{p}{e}\right)^2 2eI \quad (7)$$

For a tunnel current of ≈ 1 nA and $\kappa \approx 0.1$ nm⁻¹, $[S_F^{(BA)}] \approx 10^{-18}$ N Hz^{-1/2}, which indicates that detectable displacement noise may be generated by the tunneling electrons.

Tunneling in an atomic-scale junction is an inherently fast phenomenon with speeds greater than 1 GHz.^[79] Nevertheless, tunnel transducers as well the scanning tunneling microscopy (STM) experiments reported to date generally have low bandwidths less than 100 kHz—much slower than the speeds at which NEMS operate. These apparent bandwidth shortcomings are due to technological reasons: the impedance of a tunnel junction is quite high, on the order of GΩs; in the presence of parasitic capacitances, this results in very large RC time constants and, hence, small bandwidths.

There are, however, possibilities for useful down-conversion schemes by taking advantage of the nonlinear dependence of the tunnel current upon the tunnel gap. Intermediate frequency operation of tunnel transducers has been described previously—with applications to MEMS and surface acoustic wave (SAW) devices.^[80] In such schemes, the gap is

modulated by the motion at ω_0 of the moving surface. To detect high-frequency resonance signals, one modulates the tunnel bias voltage at $\omega_m \approx \omega_0 + \Delta\omega$. The current is a function of the bias and the gap as (see Figure 11)

$$i = \rho_S e^{-2\kappa d} [V + v(t)][1 + 2\kappa x(t) + \dots] \quad (8)$$

Hence, the term proportional to $v(t)x(t)$ will generate a signal at $\Delta\omega$, that is, within the measurement bandwidth.

4.6. Other Techniques

There are other techniques for NEMS displacement detection that are being pursued in several other laboratories. One such technique is visual monitoring inside a scanning electron microscope (SEM).^[81,82] Another technique relies on the impedance change of a quantum point contact as the nanomechanical device is flexed.^[83]

5. Summary and Outlook

Actuation of NEMS motion does not pose any significant challenges—at least in first-generation NEMS. Actuation of small displacements at high frequencies is within the reach of currently available techniques. Detection of the motion, however, is challenging. First, an unprecedented precision level is needed to read-out NEMS displacements. Compounding this problem is the high operational frequencies of NEMS. The ideal NEMS transducer must be capable of resolving extremely small displacements, across very large bandwidths.

The development of sensitive, broadband, and robust electromechanical transducers is an overarching research theme in the field of NEMS. Given that most of the methodologies from MEMS are not applicable, novel paths exploiting phenomena at the nanoscale must be explored.

Acknowledgements

Many of the ideas described herein emerged as a result of the author's collaboration with Prof. M. L. Roukes. The author also acknowledges many stimulating conversations with Dr. K. C. Schwab and Dr. A. Vandelay. The author is grateful to the US National Science Foundation for support under contracts CMS-0324416, BES-0216274, DMR-0315662, and ECS-0089061.

- [1] J. Ilene Busch-Vishniac, *Electromechanical Sensors and Actuators*, 1st ed., Springer, Berlin, **1998**.
- [2] M. L. Roukes, *Phys. World* **2001**, *14*, 25.
- [3] M. L. Roukes, *Nanoelectromechanical Systems*, Technical Digest of the 2000 Solid-State Sensor and Actuator Workshop, Hilton Head Island, SC, 6/4–8/2000, Transducer Research Foundation, Cleveland, **2000** ISBN 0–9640024–3–4, <http://arxiv.org/pdf/cond-mat/0008187>.

- [4] H. G. Craighead, *Science* **2000**, *290*, 1532.
- [5] X. M. H. Huang, C. A. Zorman, M. Mehregany, M. L. Roukes, *Nature* **2003**, *421*, 496.
- [6] K. L. Ekinci, Y. T. Yang, X. M. Huang, M. L. Roukes, *Appl. Phys. Lett.* **2002**, *81*, 2253.
- [7] K. L. Ekinci, X. M. H. Huang, M. L. Roukes, *Appl. Phys. Lett.* **2004**, *84*, 4469.
- [8] A. N. Cleland, M. L. Roukes, *Nature* **1998**, *392*, 160.
- [9] A. Erbe, H. Krömmel, A. Kraus, R. H. Blick, G. Corso, K. Richter, *Appl. Phys. Lett.* **2000**, *77*, 3102.
- [10] L. Sekaric, M. Zalalutdinov, S. W. Turner, A. T. Zehnder, J. M. Parpia, H. G. Craighead, *Appl. Phys. Lett.* **2002**, *80*, 3617.
- [11] M. L. Roukes, K. L. Ekinci, U.S. Patent 6,722,200, **2004**.
- [12] B. Ilic, H. G. Craighead, S. Krylov, W. Senaratne, C. Ober, P. Neuzil, *J. Appl. Phys.* **2004**, *95*, 3694.
- [13] N. V. Lavrik, P. G. Datskos, *Appl. Phys. Lett.* **2003**, *82*, 2697.
- [14] A. Cleland, *Foundations of Nanomechanics*, Springer, New York, **2003**.
- [15] H. M. Paynter, *Analysis and Design of Engineering Systems*, MIT Press, Cambridge, MA, **1961**.
- [16] A. Harrie, C. Tilmans, *J. Micromech. Microeng.* **1996**, *6*, 157–176.
- [17] C. V. Heer, *Statistical Mechanics, Kinetic Theory and Stochastic Processes*, Academic, New York, **1972**.
- [18] The averaging is performed over an ensemble of identical systems. Assuming the physical process giving rise to the noise is random in nature, ensemble averaging can be replaced by a long time average. See ref. [17] for as detailed discussion.
- [19] R. E. Mihailovich, J. M. Parpia, *Phys. Rev. Lett.* **1992**, *68*, 3052.
- [20] W. C. Tang, T. C. H. Nguyen, M. W. Judy, R. T. Howe, *Sens. Actuators A* **1990**, *21*, 328.
- [21] J. Soderkvist, K. Hjort, *J. Micromech. Microeng.* **1994**, *4*, 28.
- [22] M. Tortonese, R. C. Barret, C. F. Quate, *Appl. Phys. Lett.* **1993**, *62*, 834.
- [23] D. S. Greywall, B. Yurke, P. A. Busch, A. N. Pargellis, R. L. Willett, *Phys. Rev. Lett.* **1992**, *72*, 2992.
- [24] J. W. Wagner, *Phys. Acoust.* **1990**, *19*, 201.
- [25] T. G. Bifano, J. Perreault, R. K. Mali, M. N. Horenstein, *IEEE J. Sel. Top. Quantum Electron.* **1999**, *5*, 83.
- [26] Y. Martin, H. K. Wickramasinghe, *Appl. Phys. Lett.* **1987**, *50*, 1455.
- [27] R. Erlandsson, G. M. McClelland, C. M. Mate, S. Chiang, *J. Vac. Sci. Technol. A* **1988**, *6*, 266.
- [28] D. Rugar, H. J. Mamin, R. Erlandsson, J. E. Stern, B. D. Terris, *Rev. Sci. Instrum.* **1988**, *59*, 2337.
- [29] G. Meyer, N. M. Amer, *Appl. Phys. Lett.* **1988**, *53*, 2400.
- [30] P. K. Hansma, M. Longmire, J. Gurley, *J. Appl. Phys.* **1988**, *65*, 164.
- [31] R. W. Trach in MOEMS 99, Mainz, Aug. 30–Sept. 1, **1999**.
- [32] E. Ollier, *IEEE J. Sel. Top. Quantum Electron.* **2002**, *8*, 155.
- [33] P. D. Kelly, W. M. Pruessner, K. Amarnath, M. Datta, S. Kanakara-ju, C. L. Calhoun, R. Ghodssi, *IEEE Photon. Technol. Lett.* **2004**, *16*, 1412.
- [34] A. N. Cleland, M. L. Roukes, *Appl. Phys. Lett.* **1996**, *69*, 2653
- [35] H. A. Tilmans, R. Legtenberg, *Sens. Actuators A* **1994**, *45*, 67.
- [36] A. H. Nayfeh, P. F. Pai, *Linear and Nonlinear Structural Mechanics*, Wiley Interscience, **2004**.
- [37] L. Sekaric, J. M. Parpia, H. G. Craighead, T. Feygelson, B. H. Houston, J. E. Butler, *Appl. Phys. Lett.* **2002**, *81*, 4455–4457.
- [38] D. S. Greywall, B. Yurke, P. A. Busch, A. N. Pargellis, R. L. Willett, *Phys. Rev. Lett.* **1994**, *72*, 2992.
- [39] Y. T. Yang, K. L. Ekinci, X. M. H. Huang, L. M. Schiavone, M. L. Roukes, C. A. Zorman, M. Mehregany, *Appl. Phys. Lett.* **2001**, *78*, 162.
- [40] D. W. Carr, L. Sekaric, H. G. Craighead, *J. Vac. Sci. Technol. B* **1998**, *16*, 3821.
- [41] D. W. Carr, S. Evoy, L. Sekaric, A. Olkhovets, J. M. Parpia, H. G. Craighead, *Appl. Phys. Lett.* **2000**, *77*, 1545.
- [42] C. Meyer, H. Lorenz, K. Karrai, *Appl. Phys. Lett.* **2003**, *83*, 2420.
- [43] B. E. N. Keeler, D. W. Carr, J. P. Sullivan, T. A. Friedmann, J. R. Wendt, *Opt. Lett.* **2004**, *29*, 1182.
- [44] T. Kouh, D. Karabacak, D. H. Kim, K. L. Ekinci, *Appl. Phys. Lett.* **2005**, *86*, 013106.
- [45] T. R. Albrecht, P. Grütter, D. Rugar, D. P. E. Smith, *Ultramicroscopy* **1992**, *42*, 1638.
- [46] “Dielectric rectangular waveguide and directional coupler for integrated optics”: E. A. J. Marcatili, *Bell Syst. Tech. J.* **1969**, *48*, 2071–2102.
- [47] “A circular-harmonic computer analysis of rectangular dielectric waveguide”: J. E. Goell, *Bell Syst. Tech. J.* **1969**, *48*, 2133–2160.
- [48] C. Wagner, J. Frankenberger, P. P. Deimel, *IEEE Photon. Technol. Lett.* **1993**, *5*, 1257.
- [49] S. Wu, H. J. Frankena, in *SPIE Integrated Optics and Microstructures, Vol. 1793*, Boston, MA, Sept. **1992**.
- [50] E. Ollier, P. Labeye, F. Revol, in ECIO 95, Delft, The Netherlands, Apr. 3–6, **1995**.
- [51] O. Blum Spahn, C. Sullivan, J. Burkhart, C. Tigges, E. Garcia in Optical MEMS Conference, Kauai, HI, Aug. 22–24, **2000**.
- [52] S. C. Kan, T. T. H. Eng, S. S. Y. Sin, G. K. L. Wong, *Sens. Actuators A* **1996**, *54*, 679.
- [53] Y.-H. Jin, K.-S. Seo, Y.-H. Cho, S.-S. Lee, K.-C. Song, J.-U. Bu, in Optical MEMS Conference, Kauai, HI, Aug. 22–24, **2000**.
- [54] J. S. Foresi, P. R. Villeneuve, J. Ferrara, E. R. Thorn, G. Steinmeyer, S. Fan, J. D. Joannopoulos, L. C. Kimerling, H. I. Smith, E. P. Ippen, *Nature* **1997**, *390*, 143.
- [55] J. S. Foresi, M. R. Black, A. M. Agarwal, L. C. Kimerling, *Appl. Phys. Lett.* **1996**, *68*, 2052.
- [56] J. P. R. Lacey, F. P. Payne, *IEEE Proc.* **1990**, *137*, 282.
- [57] V. Van, P. Philippe Absil, J. V. Hryniewicz, P.-T. Ho, *J. Lightwave Technol.* **2001**, *19*, 1734.
- [58] K. K. Lee, D. R. Lim, H.-C. Luan, A. Agarwal, J. Foresi, L. C. Kimerling, *Appl. Phys. Lett.* **2000**, *77*, 1617.
- [59] P. A. Truitt, J. Hertzberg, K. C. Schwab, *Bull. Am. Phys. Soc.*, in press.
- [60] M. D. LaHaye, O. Buu, B. Camarota, K. C. Schwab, *Science* **2004**, *304*, 74.
- [61] R. G. Knobel, A. N. Cleland, *Nature* **2003**, *424*, 291.
- [62] P. M. Blencowe, *Proc. SPIE-Int. Soc. Opt. Eng.* **2003**, *5115*, 64.
- [63] P. M. Blencowe, N. M. Wybourne, *Appl. Phys. Lett.* **2000**, *77*, 3845.
- [64] Tai-Ran Hsu, *MEMS and Microsystems: Design and Manufacture*, McGraw Hill, **2002**.
- [65] R. G. Beck, M. A. Eriksson, R. M. Westervelt, *Appl. Phys. Lett.* **1998**, *73*, 1149.
- [66] R. Knobel, A. N. Cleland, *Appl. Phys. Lett.* **2002**, *81*, 2258.
- [67] T. W. Kenny, W. J. Kaiser, J. K. Reynolds, J. A. Podosek, H. K. Rockstad, E. C. Vote, S. B. Waltman, *J. Vac. Sci. Technol. A* **1992**, *10*, 2114.
- [68] J. Tersoff, in *Scanning Probe Microscopy and Spectroscopy* (Ed.: D. Bonnell), Wiley, New York, **2000**.
- [69] M. F. Bocko, *Rev. Sci. Instrum.* **1990**, *61*, 3763.
- [70] M. F. Bocko, K. A. Stephenson, R. H. Koch, *Phys. Rev. Lett.* **1988**, *61*, 726.
- [71] C. Presilla, R. Onofrio, M. F. Bocko, *Phys. Rev. B* **1992**, *45*, 3735.
- [72] D. Mozyrsky, I. Martin, *Phys. Rev. Lett.* **2002**, *89*, 018301.
- [73] A. D. Armour, M. P. Blencowe, Y. Zhang, *Phys. Rev. B* **2004**, *69*, 125313.
- [74] J. Casas-Vazquez, D. Jou, *Rep. Prog. Phys.* **2003**, *66*, 1937.
- [75] N. F. Schwabe, A. N. Cleland, M. C. Cross, M. L. Roukes, *Phys. Rev. B* **1995**, *52*, 12911.
- [76] B. Yurke, G. P. Kochanski, *Phys. Rev. B* **1990**, *41*, 8184.

- [77] A. A. Clerk, S. M. Girvin, *Phys. Rev. B* **2004**, 70, 121303(R).
- [78] A. Y. Smirnov, L. G. Mourokh, N. J. M. Horing, *Phys. Rev. B* **2003**, 67, 115312.
- [79] G. Nunes, Jr., M. R. Freeman, *Science* **1993**, 262, 1029.
- [80] E. Chilla, W. Rohrbeck, H.-J. Fröhlich, R. Koch, K. H. Rieder, *Appl. Phys. Lett.* **1992**, 61, 3107–3109.
- [81] D. A. Dikin, X. Chen, W. Ding, G. Wagner, R. S. Ruoff, *J. Appl. Phys.* **2003**, 93, 226.
- [82] Y. Zhu, N. Moldovan, H. D. Espinosa, *Appl. Phys. Lett.* **2005**, 86, 013506.
- [83] A. N. Cleland, J. S. Aldridge, D. C. Driscoll, A. C. Gossard, *Appl. Phys. Lett.* **2002**, 81, 1699.

Received: March 8, 2005

Published online on July 1, 2005